

# Phase-Based Approaches for Rapid Construction of Magnetic Fields in NV Magnetometry

Prabhat Anand\*, Ankit Khandelwal\*, Achanna Anil Kumar\*, M Girish Chandra\*, Pavan K Reddy\*,  
Anuj Bathla<sup>‡</sup>, Dasika Shishir<sup>†</sup>, Kasturi Saha<sup>†§¶</sup>

\*TCS Research, Tata Consultancy Services Ltd, Bengaluru, India

{prabhat.prabhat, khandelwal.ankit3, achannaanil.kumar, m.gchandra, pavank.reddy}@tcs.com

<sup>†</sup>Department of Electrical Engineering, Indian Institute of Technology Bombay (IITB), Mumbai, India

<sup>‡</sup>Centre for Research in Nanotechnology and Science (CRNTS), Department of Electrical Engineering, IITB, India

<sup>§</sup>Centre of Excellence in Quantum Information, Computing Science and Technology, IITB, India

<sup>¶</sup>Centre of Excellence in Semiconductor Technologies (SemiX), IITB, India

{bathla.anuj, dshishir}@iitb.ac.in, kasturis@ee.iitb.ac.in

**Abstract**—With the second quantum revolution underway, quantum-enhanced sensors are moving from laboratory demonstrations to field deployments, providing enhanced and even new capabilities. Signal processing and operational software are becoming integral parts of these emerging sensing systems to reap the benefits of this progress. This paper looks into widefield Nitrogen Vacancy Center-based magnetometry and focuses on estimating the magnetic field from the Optically Detected Magnetic Resonances (ODMR) signal, a crucial output for various applications. Mapping the shifts of ODMR signals to phase estimation, a computationally efficient Fourier Transform-based approach is proposed, which also involves linear curve fit and Estimation of Signal Parameters via Rotational Invariant Techniques (ESPRIT) as additional steps. The existing methods in the quantum sensing literature take different routes for determining magnetic field maps. To showcase the functionality and effectiveness of the suggested technique, relevant results, based on experimental data are provided, which shows a significant reduction in computational time with the proposed method over existing method.

**Index Terms**—Quantum Sensors, Nitrogen Vacancy Centers, Magnetometry, Fourier Transform, Phase, ESPRIT

## I. INTRODUCTION

It is widely believed that continuous advances in modern science and technology rely heavily on precise sensing and atomic level magnetism control [1]. A very promising quantum sensing approach, signifying the progression from fundamental research to practical application, is based on the negatively charged nitrogen vacancy (NV) centers in the diamond crystal [2]–[4]. They provide high magnetic sensitivity in ambient conditions with large dynamic range and high spatial resolution [2]. This technology can be applied to efficiently measure temperature, electric and magnetic fields, and pressure. The magnetic field detection of the NV centers relies on the magnetic interaction of the electron spin via the Zeeman effect [4], [5]. The NV spin state can be optically initialized, suitably governed using Microwave (MW) fields, and read out optically with extended coherence periods [2].

The advancement of magnetic sensor technology that can simultaneously achieve both high magnetic sensitivity and high spatial resolution is becoming increasingly vital across a variety of fields, from solid-state physics to life sciences [1],

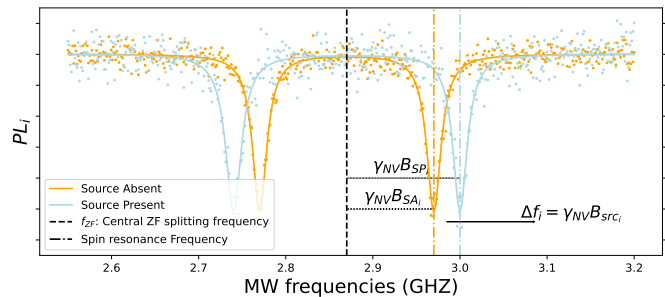


Fig. 1. A typical ODMR has PL recorded over a band of MW frequencies. Here, two ODMRs for a single  $i^{th}$  NV axis are shown in the presence and absence of a magnetic source demonstrating magnetic field-dependent shifts in resonant frequencies; elaborated in (2).

[2], [6]. For the work presented here, we consider a widefield magnetometer consisting of an ensemble of NV centers, that is, a dense layer of NV centers induced near the surface of diamond [7]. A typical widefield experimental setup can be seen in [8, Fig.2.11] and in [7, Fig.1]. One of the important steps for many applications involving NV magnetometry is a good construction of 2D maps of 3D vectorial magnetic fields [9]. Each pixel value of these maps is typically determined from the ODMR “signal” (Fig. 1). The characteristic ODMR in widefield imaging mode is produced when red photoluminescence (PL) of NV-ensembles is recorded by a conventional scientific camera (say, Charge Coupled Device (CCD) camera) in the presence of a MW field with varying frequencies [7]. Each frequency step results in a different 2D frame of PL, and for each pixel, the values in the consecutive frames put together result in the ODMR signal, which is basically a signal in the frequency domain. A popular way of measuring the magnetic field of a source is by tracking the shifts in the resonant frequency of the ODMR signals in the presence and absence of the source [6], [7]. With appropriate processing, a precise imaging of the 3D magnetic field is possible.

There are different propositions [6], [8], in the existing literature to process ODMR signal to construct magnetic maps. It is important to note at this juncture that the measured ODMR signal suffers from different distortions and noise corruption [10]–[14]. There is also an effect due to the separation between

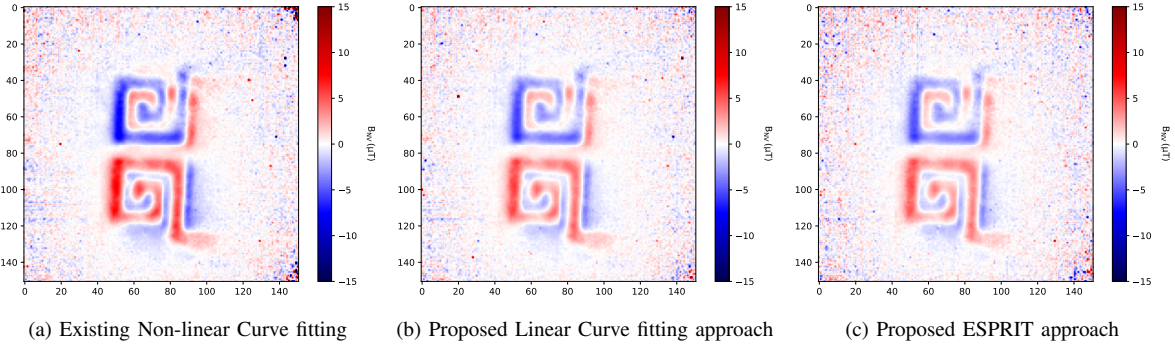


Fig. 2. Construction of one component of Magnetic Field from ODMR: (a) The TRF algorithm implemented in scipy is used to fit a Lorentzian. (b) FFT-based phase determination incorporating linear curve fit is used. (c) FFT-based phase determination incorporating ESPRIT is used.

the magnetic source and the NV-induced diamond slab plane, known as stand-off distance. Viewing from a signal processing perspective one can think of an “ideal” ODMR signal passing through a system that introduces artifacts which is further affected by noise. This opens up a relatively new territory for the signal-processing community to contribute to the exciting area of quantum-enhanced sensing.

In this paper in Section II, we propose a novel technique by adopting methods of signal processing and suitably modifying them to arrive at a way to construct a magnetic field from the ODMR signal. Such an approach does not exist in the context of quantum sensing literature to the best of our knowledge. The relevant results captured in Section III demonstrate the applicability and usefulness of the technique including  $\sim 70\times$  improvement in processing speed compared to the existing method on a real data.

## II. MAGNETIC FIELD CONSTRUCTION FROM ODMR

As the physics and technological advancements of NV-center based magnetometry have been extensively documented in other works [2], [8], [15], [16], this paper will not address those topics. Restricting to the ODMR signal, Fig. 1 depicts data points of a section of a typical ODMR signal. In absence of any magnetic field, NV centers have a degenerate excited state having an energy gap, corresponding to roughly  $f_{ZF} = D_{gs} = 2.87$  GHz, called zero-field (ZF) splitting frequency (see Fig. 1) giving a single dip in ODMR centered around it. The number of dips increases in the presence of magnetic field with every two dips centered around one of the four magnetic field component ( $B_{NV_i}$ )-dependent resonant frequencies  $f_i$  given in (1). Once this intensive task of determining the central frequencies  $f_i$  is done from the ODMR, by tracking these changes in  $f_i$ , one can determine changes in the external fields. Hence, two sets of measurements are carried out for magnetic field construction (1), that is, an MW frequency sweep is carried out in the absence of any sample (SA) when  $B_{NV_i} = B_{SA_i}$  and is subtracted from  $B_{NV_i} = B_{SP_i}$  that is measured in the presence of the magnetic sample (SP) (2).

$$\begin{aligned} \Delta f_i &= |f_{SP_i} - f_{SA_i}| \\ &= |(D_{gs} + \gamma_{NV} B_{SP_i}) - (D_{gs} + \gamma_{NV} B_{SA_i})| \\ &= |\gamma_{NV} (B_{SP_i} - B_{SA_i})| = \gamma_{NV} B_{src_i} \end{aligned} \quad (1)$$

$$\text{given } B_{SP_i} = B_{bias_i} + B_{src_i}, \quad B_{SA_i} = B_{bias_i} \quad (2)$$

where  $B_{bias_i}$  is bias magnetic field and  $B_{src_i} (\ll B_{bias_i})$  is magnetic field due to source along  $i^{th}$  NV axis,  $i \in \{1, 2, \dots, 8\}$  and  $\gamma_{NV} (= 28 \text{ kHz}/\mu\text{T})$  is the gyromagnetic ratio of NV center, a fundamental constant. The challenge however is to precisely determine the central frequency  $f_i$ .

### A. Few Remarks on Existing Methodologies

*Lorentzian-fitting Approach (LF):* To determine the central frequency of the dip in ODMR, typically Lorentzian (3) is fitted onto the full ODMR spectrum acquired, due to prevalence of Lorentzian broadening in Continuous-wave-ODMR [17], using different multi-parameter optimization algorithms.

$$f(\nu) = 1 - \sum_{i=1}^8 C_i \left( \frac{\gamma^2}{4(\nu_i - \nu)^2 + \gamma^2} \right) \quad (3)$$

From this non-linear fitting, one can obtain the values of central frequencies which, in turn, give the value of external magnetic field using (2). A variation to this method, where the slope of Lorentzian is fitted, can be found in [7]. In the following section, we propose an alternative efficient approach based on signal processing methods.

### B. Proposed approach: Fourier Transform based approach

In this section, we propose an alternative, computationally efficient approach based on Fourier Transform (FT) to estimate the magnetic field  $B_{src_i}$ . From now onwards, we consider a portion of full ODMR around a single resonant frequency. Let  $F_{SA}(f)$  and  $F_{SP}(f)$  denote the ODMR with source absent and source present respectively (Fig. 1). Now,  $F_{SP}(f)$  can be visualized, from a theoretical point of view, as *frequency shifted signal* of  $F_{SA}(f)$  by  $B_{src_i}$ . The actual experimental data brings some dissimilarity among the signals, but even then shifted property is a good first approximation. Hence, we can express  $F_{SP}(f) = F_{SA}(f - \Delta f_i) = F_{SA}(f - \gamma_{NV} B_{src_i})$ . Let the inverse FT [18] (IFT) of  $F_{SA}(f)$ ,  $\mathcal{F}^{-1}(F_{SA}(f)) = f_{SA}(t)$ . Using the identities of IFT [18],  $f_{SP}(t) = \mathcal{F}^{-1}(F_{SP}(f))$  can be expressed as

$$f_{SP}(t) = f_{SA}(t) e^{j2\pi t \Delta f_i}. \quad (4)$$

Note that  $f_{SA}(t)$  can easily be found as the ODMR  $F_{SA}(f)$  is measurable without the source, hence

$$f_{B_{src_i}}(t) = \frac{f_{SP}(t)}{f_{SA}(t)} = e^{j2\pi t \Delta f_i}. \quad (5)$$

Notice that the unknown  $\Delta f_i = \gamma_{NV} B_{src_i}$  resides in the phase of  $f_{B_{src}}(t)$ . Also, note from Fig. 1, that  $F_{SA}(f)$  is a slowly varying signal and hence  $f_{SA}(t)$  is a lowpass signal in the time domain with most of the energy concentrated at the *low-time* band region (analogous to standard low-frequency band signal). Hence, before further processing we filter the signal as  $f_{B_{src}}^{(filt)}(t) = f^{(filt)}(t)f_{B_{src}}(t)$ , where  $f^{(filt)}(t)$  is defined as

$$f^{(filt)}(t) = \begin{cases} 1, & t \in [-T_t, +T_t] \\ 0, & \text{otherwise} \end{cases} \quad (6)$$

We now use the following two approaches to estimate  $B_{src_i}$  from  $f_{B_{src}}^{(filt)}(t)$ .

1) *Line-fitting based approach*: We first unwrap  $f_{B_{src}}^{(filt)}(t)$ , which can be expressed as

$$g(t) = -j \ln(f_{B_{src}}^{(filt)}(t)) = 2\pi t \gamma_{NV} B_{src_i}. \quad (7)$$

We then do line-fitting for the measurements  $g(t)$  in the region  $t \in [-T_t, +T_t]$  using the simple least squares approach. The slope of this line shall provide an estimate of  $B_{src_i}$ .

2) *Super-resolution: ESPRIT approach*: Observing that estimating  $f_{B_{src}}^{(filt)}(t)$  is akin to a complex frequency estimation (see (5)), we also propose to employ a super-resolution techniques like ESPRIT [19] to obtain  $B_{src_i}$ .

### C. Comparison between LF and FT approaches

Notice from (5), the existing LF-based approach requires a computationally intensive curve-fitting of a non-linear multivariate function. Bypassing this, in the proposed approach requires FT computation of ODMR functions, which in practice, can be computed using the efficient FFT techniques. Further, uni-variate linear line-fitting approach is computationally very efficient. The super-resolution approach, on the other hand is slightly more computationally complex compared to line-fitting approach as it requires eigenvalue decomposition [19]. However, as shall be shown later in Section III on real data, both the proposed approaches are much quicker without any performance loss.

## III. RESULTS & DISCUSSION

Two ODMRs with sampling rate of 100 kHz about a single resonant frequency, obtained experimentally from the setup described in [7], were utilised in studying and evaluating the proposed techniques. Both the techniques were implemented using built-in functions of scipy [20]. We used the time filter width  $T_t = 4$  samples, and a threshold of  $15\mu T$  and  $-15\mu T$ . Further a Median Filtering was used on top of it to get the final constructed  $B_{src}$  shown in Fig. 2. Fig. 2a, 2b and 2c shows the construction using the existing LF-based, the proposed FT based linear curve fitting and proposed FT based ESPRIT based approaches respectively. Here, we employed the Trust Region Reflective (TRF) algorithm [21] for LF based non-linear curve fitting approach. From the figures, one can notice similar construction using all the three methods. However, our implementation of FT based techniques took  $\sim 70\times$  lesser

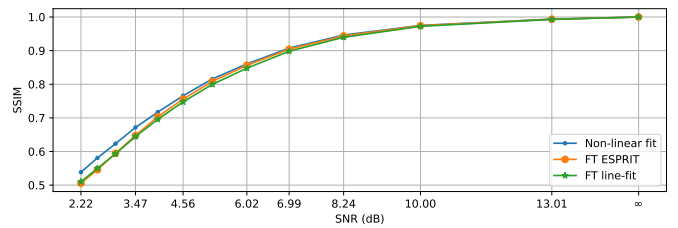


Fig. 3. Robustness against the addition of noise: Zero-mean Gaussian noise was added in the ODMR with varying Signal-to-Noise ratio (SNR) and a magnetic field map was produced. This map was compared to the magnetic field map obtained using the original ODMR signal using the respective method.

time than that of LF based method. This huge reduction can be attributed to the efficient computation of FT using FFTs and requiring only a simple line-fitting unlike the existing LF based approach. Note that as mentioned previously, while the proposed ESPRIT approach requires eigenvalue decomposition, since only 8 samples are considered (time-width =  $2T_t$ ), the increase in complexity compared to the proposed line-fitting approach is marginal and both the proposed approaches yielded results in almost similar time.

The techniques were further tested for robustness against noise by adding suitable Gaussian noise corresponding to different SNRs. The images generated from these noisy ODMRs are compared with the original images constructed through corresponding techniques using structural similarity index measure (SSIM) [22] which are plotted in Fig. 3. The similarity measure improves as SNR increases with more or less similar characteristics, thus validating an equal robustness of existing LF based and the proposed FT-based approaches.

The results hence demonstrates similar performance of the existing and proposed approaches, however with a significant reduction in the computational time, thus making the proposed approach attractive for magnetic field construction from ODMR in NV magnetometry.

## IV. CONCLUSION

NV center-based magnetometry is emerging as a useful technology with different applications. Determining accurate magnetic field maps is one of the important intermittent outputs in the analytics pipeline to carry out the inference relevant to the concerned application. It is interesting to see many of the modules through a signal-processing lens and arrive at useful algorithms/techniques not only for NV magnetometry but also for different quantum sensing systems. This paper proposed a computationally faster technique to construct the magnetic field by bundling some of the techniques regularly used in the signal processing community; an advantage possibly benefiting the development of portable versions of the magnetometers. Driven by this, immense possibility is seen to consider different signal processing techniques not only for magnetic field construction but also for other modules in the pipeline for the application at hand. For instance, one can look into the inverse problem of current reconstruction from the magnetic field maps to charge flow in semiconductor chips, which is useful for different purposes.

## REFERENCES

- [1] M. Lee, J. Yoon, and D. Lee, "Atomic scale magnetic sensing and imaging based on diamond nv centers," in *Magnetometers*, S. Curilef, Ed. Rijeka: IntechOpen, 2019, ch. 4. [Online]. Available: <https://doi.org/10.5772/intechopen.84204>
- [2] J. R. Maze *et al.*, "Nanoscale magnetic sensing with an individual electronic spin in diamond," *Nature*, vol. 455, no. 7213, pp. 644–647, Oct 2008. [Online]. Available: <https://doi.org/10.1038/nature07279>
- [3] P. Kehayias, "High-resolution magnetic microscopy applications using nitrogen-vacancy centers in diamond," 9 2021. [Online]. Available: <https://www.osti.gov/biblio/1826099>
- [4] F. M. Stürner *et al.*, "Integrated and portable magnetometer based on nitrogen-vacancy ensembles in diamond," *Advanced Quantum Technologies*, vol. 4, no. 4, p. 2000111, 2021. [Online]. Available: <https://onlinelibrary.wiley.com/doi/abs/10.1002/qute.202000111>
- [5] J. F. Barry *et al.*, "Sensitivity optimization for nv-diamond magnetometry," *Rev. Mod. Phys.*, vol. 92, p. 015004, Mar 2020. [Online]. Available: <https://link.aps.org/doi/10.1103/RevModPhys.92.015004>
- [6] F. Casola, T. van der Sar, and A. Yacoby, "Probing condensed matter physics with magnetometry based on nitrogen-vacancy centres in diamond," *Nature Reviews Materials*, vol. 3, no. 1, p. 17088, Jan 2018. [Online]. Available: <https://doi.org/10.1038/natrevmats.2017.88>
- [7] M. Parashar, A. Bathla, D. Shishir, A. Gokhale, S. Bandyopadhyay, and K. Saha, "Sub-second temporal magnetic field microscopy using quantum defects in diamond," *Scientific Reports*, vol. 12, no. 1, p. 8743, May 2022. [Online]. Available: <https://doi.org/10.1038/s41598-022-12609-3>
- [8] M. Garsi, "OPUS: Optimising nitrogen-vacancy based widefield imaging for broadband applications — dx.doi.org," <http://dx.doi.org/10.18419/opus-13834>, 2023, [Accessed 16-06-2024].
- [9] B. J. Maertz, A. P. Wijnheijmer, G. D. Fuchs, M. E. Nowakowski, and D. D. Awschalom, "Vector magnetic field microscopy using nitrogen vacancy centers in diamond," *Applied Physics Letters*, vol. 96, no. 9, p. 092504, 03 2010. [Online]. Available: <https://doi.org/10.1063/1.3337096>
- [10] Y. Li *et al.*, "Noise suppression of nitrogen-vacancy magnetometer in lock-in detection method by using common mode rejection," *Micromachines*, vol. 14, no. 10, 2023. [Online]. Available: <https://www.mdpi.com/2072-666X/14/10/1823>
- [11] P. Frontera, S. Alessandrini, and J. Stetson, "Shipboard calibration of a diamond nitrogen vacancy magnetic field sensor," in *2018 IEEE/ION Position, Location and Navigation Symposium (PLANS)*. IEEE, 2018, pp. 497–504.
- [12] J. Zhang *et al.*, "A modified spin pulsed readout method for nv center ensembles reducing optical noise," *IEEE Transactions on Instrumentation and Measurement*, vol. 69, no. 7, pp. 4370–4378, 2020.
- [13] J. L. Webb *et al.*, "Nanotesla sensitivity magnetic field sensing using a compact diamond nitrogen-vacancy magnetometer," *Applied Physics Letters*, vol. 114, no. 23, p. 231103, 06 2019. [Online]. Available: <https://doi.org/10.1063/1.5095241>
- [14] L. Troise *et al.*, "Laser stimulation of muscle activity with simultaneous detection using a diamond colour centre biosensor," 2021.
- [15] M. W. Doherty, N. B. Manson, P. Delaney, F. Jelezko, J. Wrachtrup, and L. C. Hollenberg, "The nitrogen-vacancy colour centre in diamond," *Physics Reports*, vol. 528, no. 1, p. 1–45, Jul. 2013. [Online]. Available: <http://dx.doi.org/10.1016/j.physrep.2013.02.001>
- [16] G. Balasubramanian *et al.*, "Ultralong spin coherence time in isotopically engineered diamond," *Nature Materials*, vol. 8, no. 5, pp. 383–387, May 2009. [Online]. Available: <https://doi.org/10.1038/nmat2420>
- [17] K. Jensen, V. M. Acosta, A. Jarmola, and D. Budker, "Light narrowing of magnetic resonances in ensembles of nitrogen-vacancy centers in diamond," *Phys. Rev. B*, vol. 87, p. 014115, Jan 2013. [Online]. Available: <https://link.aps.org/doi/10.1103/PhysRevB.87.014115>
- [18] M. Vetterli, J. Kovačević, and V. K. Goyal, *Foundations of signal processing*. Cambridge University Press, 2014.
- [19] T. K. Moon and W. C. Stirling, "Mathematical methods and algorithms for signal processing," (*No Title*), 2000.
- [20] P. Virtanen *et al.*, "SciPy 1.0: Fundamental Algorithms for Scientific Computing in Python," *Nature Methods*, vol. 17, pp. 261–272, 2020.
- [21] M. A. Branch, T. F. Coleman, and Y. Li, "A subspace, interior, and conjugate gradient method for large-scale bound-constrained minimization problems," *SIAM Journal on Scientific Computing*, vol. 21, no. 1, pp. 1–23, 1999. [Online]. Available: <https://doi.org/10.1137/S1064827595289108>
- [22] Z. Wang, A. Bovik, H. Sheikh, and E. Simoncelli, "Image quality assessment: from error visibility to structural similarity," *IEEE Transactions on Image Processing*, vol. 13, no. 4, pp. 600–612, 2004.